On the analysis of canvas wrinkling via isogeometric stereocorrelation

John-Eric Dufour, Emilie Gonnet, Sébastien Grau, François Hild

On the analysis of canvas wrinkling via isogeometric stereocorrelation

John-Eric Dufour[a], Emilie Gonnet[b], Sébastien Grau[b], François Hild[a,*]

[a] *LMT-Cachan, ENS Cachan / CNRS / Université Paris-Saclay*
61 avenue du Président Wilson, 94235 Cachan Cedex, France
[b] *Ecole de Condé, 7-9 rue Cambronne, 75015 Paris, France*

Abstract

Wrinkling is to be avoided in the restoration of works on canvas. In the worst cases, it may lead to paint cracking. Visual rendering of the paint may also change because of such mechanism. It is proposed to measure wrinkling under various conditions of contrast and loading *via* isogeometric stereocorrelation. This method allows low contrasted paints to be analyzed in addition to very large deformations that occur in punch tests on canvas.

Keywords: Climatic chamber, Optical technique, Punch test, Restoration, Wrinkling

1. Introduction

The restoration and transport of works on canvas requires their mechanical behavior to be understood as best as possible to avoid any damage. Further, in many cases, canvasses are not stress-free and thus very sensitive to the environment (*e.g.,* relative humidity (Berger and Russel, 1994; Malowany et al., 2014)) in which they are stored and exhibited (*e.g.,* museums, places of gathering). Being part of the cultural heritage, these works are handled with special care and the understanding of their deformations during these stages is very important. Over the last decades, non-destructive and possibly non-contacting

*Corresponding author
Email address: hild@lmt.ens-cachan.fr (François Hild)

techniques have been proposed to help the restoration of various works (James et al., 1983; Dulieu-Barton et al., 2005; Ambrosini et al., 2008; Mudge et al.; Remondino et al., 2011; Gavrilov et al., 2014; Sfarra et al., 2014). Among various optical techniques that are utilized to monitor the 3D shape and deformation of canvasses, stereocorrelation is easy-to-implement and will be used herein.

One critical issue associated with stereocorrelation is to have sufficient image contrast to enable the registration to succeed (Khennouf et al., 2010; Dureisseix et al., 2011). If natural contrast is not sufficient, *ad hoc* procedures may be considered, for instance, by projecting a random pattern in addition to the negative image of the original surface (Dureisseix et al., 2011). This method allows 3D shapes to be measured. However, it does not enable 3D surface motions to be evaluated. An alternative route consists of working on model canvas paintings (Malowany et al., 2014) for which random speckle patterns (*i.e., à la* Roy Lichtenstein) are deposited onto the observed surfaces as classically performed in mechanical engineering (Sutton, 2013). 3D shapes and surface displacements can then be measured via stereocorrelation (also referred to as 3D digital image correlation or StereoDIC (Sutton et al., 2009)).

The aim of the present work is to use *global* approaches to stereocorrelation (Beaubier et al., 2014; Dufour et al., 2015a; Dubreuil et al., 2016), which consist of measuring 3D shapes and surface displacements when registrations are performed over the whole surface of interest and not locally as in the aforementioned approaches (Khennouf et al., 2010; Dureisseix et al., 2011; Malowany et al., 2014). Consequently, if some contrasted zones exist, the shape and displacement interpolations will allow the sought information to be assessed everywhere. Further, since wrinkling is monitored, the use of higher order displacement interpolations (*e.g.,* provided by non uniform rational B-splines or NURBS (Piegl and Tiller, 1997)) is desirable. To prove the feasibility of isogeometric stereocorrelation, two test cases are analyzed. First, the effect of relative humidity variations will be studied for model canvas paintings and the *Descent of the Cross*, which was recently restored and attributed to the Swiss painter Sebastian Düring (1671-1723) (Grau, 2014). For the actual work, the

raw painted face will be analyzed (*i.e.,* no speckle pattern was applied). Second, a punch test on modern canvas will be studied. This test is very challenging since very large out-of-plane motions occur. A new enrichment strategy will be implemented in the NURBS framework used herein to measure 3D shapes and their motions.

The outline of the paper is as follows. The main principles of isogeometric stereocorrelation are introduced in Section 2. Section 3 deals with the analysis of canvasses under different relative humidity levels. The first part is devoted to the study of two model canvas paintings with different tensioning systems to minimize wrinkling. The second part then applies the best tensioning system to the restoration of the *Descent of the Cross*. Last, Section 4 is devoted to a punch test on canvas nailed on its frame. It required the NURBS-based kinematic basis to be gradually enriched to properly measure the complex deformation with numerous wrinkles.

2. Isogeometric stereocorrelation

Isogeometric stereocorrelation is a global approach based upon the gray level conservation between multiple images of the same object (Dufour et al., 2015b). The stereo-rig, which is usually composed of 2 cameras, first needs to be calibrated (Sutton et al., 2009). This calibration procedure can be performed using different methods, namely, with a planar calibration target (Lucas and Kanade, 1981; Faugeras and Toscani, 1987; Weng et al., 1992; Zhang, 2000; Salvi et al., 2002) or with the object of interest itself (Faugeras et al., 1992; Fusiello, 2000; Beaubier et al., 2014). In the present case two different strategies will be followed. First, the easel onto which painted works will be put will serve as calibration target. Second, an open book target will also be considered (Besnard et al., 2010) in the punch test. The reason for choosing such calibration targets is related to the fact that only one pair of pictures will be used during this step.

2.1. Surface model

In global stereocorrelation, there are two ways of defining the surface of interest. First low order shape functions may be considered (*e.g.,* meshes made of triangular (Dubreuil et al., 2016) or quadrilateral (Dufour et al., 2014) elements). Second higher order interpolations may be considered (*e.g.,* Bézier or NURBS patches (Beaubier et al., 2014; Dufour et al., 2015a)). Since wrinkling requires higher order interpolations of the measured displacement fields, the technique used herein is isogeometric stereocorrelation, namely, the surface of interest is described by NURBS patches.

The three-dimensional shape $\boldsymbol{X} = (X, Y, Z)$ of an external surface is written as $\boldsymbol{X}(\boldsymbol{\xi})$, where $\boldsymbol{\xi} = (u, v)$ define the parametric space, conventionally spanning the elementary square $[0, 1]^2$. What is assumed to be known is the virtual (or nominal) shape of the object of interest. A NURBS patch is defined by its order, a network of control points with associated weights, and its knot vector (Piegl and Tiller, 1997). The surface $\boldsymbol{X}(u, v) = (X, Y, Z)$ is expressed in the parametric space (u, v) as

$$\boldsymbol{X}(u,v) = \sum_{i=0}^{m}\sum_{j=0}^{n} B_{ij}(u,v)\boldsymbol{P_{ij}} \tag{1}$$

where the blending functions are defined as

$$B_{ij}(u,v) = \frac{N_{i,p}(u)N_{j,q}(v)\omega_{ij}}{\sum_{i=0}^{m}\sum_{j=0}^{n} N_{i,p}(u)N_{j,q}(v)\omega_{ij}} \tag{2}$$

with

$$\forall u \in [0,1], N_{i,0}(u) = \begin{cases} 1 \text{ when } u_i \leq u \leq u_{i+1} \\ 0 \text{ otherwise} \end{cases} \tag{3}$$

and

$$N_{i,p}(u) = \frac{u - u_i}{u_{i+p} - u_i} N_{i,p-1}(u) + \frac{u_{i+p+1} - u}{u_{i+p+1} - u_{i+1}} N_{i+1,p-1}(u) \ , \tag{4}$$

where $N_{i,p}$ are mixing functions, $\boldsymbol{P}_{ij}$ the coordinates of control points of the surface, ω_{ij} the corresponding weights, $(m+1) \times (n+1)$ the number of control points and (p, q) the degrees of the surface.

2.2. Calibration and 3D shape measurements

This first part of a stereocorrelation analysis consists of a two-step procedure. First the camera parameters are estimated (*i.e.,* the projection matrices that link any 3D point to its 2D coordinates in the camera plane). Second the observed shape is measured according to its mathematical description (Beaubier et al., 2014).

The calibration procedure consists in determining the elements of the projection matrices. Stereomatching is written as the minimization of the sum of squared differences with respect to the elements of the projection matrices (Beaubier et al., 2014)

$$\eta^2_{tot}([\boldsymbol{M^{c_1}}],[\boldsymbol{M^{c_2}}]) = \sum_{ROI} \left(f^{c_1}(\boldsymbol{\xi},[\boldsymbol{M^{c_1}}]) - f^{c_2}(\boldsymbol{\xi},[\boldsymbol{M^{c_2}}])\right)^2 \tag{5}$$

where $[\boldsymbol{M^{c_i}}]$ denotes the projection matrix of the i-th camera, and f^{c_i} the image of the reference configuration shot by the i-th camera. A Gauss-Newton algorithm is used to perform the nonlinear least squares minimization.

Once the projection matrices are known, the mathematical model of the observed surface is updated by moving the control points. Stereomatching is performed again by minimizing the sum of squared differences

$$\eta^2_{tot}(\{\boldsymbol{P}\}) = \sum_{ROI} \left(f^{c_1}(\boldsymbol{\xi},\{\boldsymbol{P}\}) - f^{c_2}(\boldsymbol{\xi},\{\boldsymbol{P}\})\right)^2 \tag{6}$$

with respect to the control point positions, which are all gathered in the column vector $\{\boldsymbol{P}\}$. A Gauss-Newton algorithm is used again to perform the nonlinear least squares minimization.

2.3. 3D displacement measurement

When the observed 3D shape has been determined, displacement measurements are performed to evaluate the surface deformation during various experiments on model canvas paintings (see Sections 3 and 4), or for monitoring purposes of a work restoration (see Section 3.5). In the following, the kinematic

basis is also NURBS-based, namely, the displacement of any point of the surface is obtained by moving the control points, which will deform the surface according to the chosen parameterization.

The stereocorrelation functional becomes (Dufour et al., 2015b)

$$\eta^2(\{\mathrm{d}\boldsymbol{P}\}) = \sum_{i=1}^{2} \sum_{ROI} \left(g^{c_i}(\boldsymbol{\xi}, \{\boldsymbol{P} + \mathrm{d}\boldsymbol{P}\}) - f^{c_i}(\boldsymbol{\xi}, \{\boldsymbol{P} + \mathrm{d}\boldsymbol{P}\})\right)^2 \tag{7}$$

and is minimized via Gauss-Newton scheme with respect to the parameterization of the displacement field $\{\mathrm{d}\boldsymbol{P}\}$ of the control points for each considered time. g^{c_i} denotes the image of the deformed configuration shot by the i-th camera. The interested reader will find additional details on such isogeometric approaches in (Beaubier et al., 2014; Dufour et al., 2015a,b).

3. Restoration of the *Descent of the Cross*

The first case study is associated with the restoration of the *Descent of the Cross* (Saint-Maurice basilica, Switzerland, see Figure 1) for which the tensioning system had to be studied (Grau, 2014). Its size is 56.3×75.3 cm. Due to significant humidity variations in the basilica, the canvas tension varied and may lead to wrinkles that are detrimental to the visual quality of the work and its aging. Two tensioning systems have been investigated on mockups (*i.e.,* model canvas paintings) that were submitted to humidity variations. The 3D shapes and motions were measured via isogeometric stereocorrelation. Once the system was implemented on the *Descent of the Cross* painting, its 3D shape and motions were also monitored via isogeometric stereocorrelation to validate the chosen technical solution.

Figure 1: Front (top) and back (bottom) faces of the *Descent of the Cross* prior to (left) and after (right) restoration. The size of the work is 56.3×75.3 cm

3.1. Conservation conditions

Exhibition of paintings on canvas often means dealing with rather severe environmental conditions. In the present case, the painting undergoes humidity and temperature variations over various seasons since the temperature is controlled by the central heating system of the basilica. The change of relative humidity and temperature is shown in Figure 2 when the thermohygrometer (KlimaLogg Pro®, standard relative humidity resolution: 1 %, standard tem-

perature resolution: 0.1 °C) was located exactly where the work is exhibited. The recorded data spanned from September 7, 2013 to October 13, 2014. For the analyzed 401 days the relative humidity varied between 77 % and 30 % (with a mean level of 58 %). Meanwhile the mean temperature was equal to 18.7 °C (with a standard deviation of 1.6 °C). The spikes in the reported data correspond to instants of time when the heating system was turned off and on. From these data it is concluded that the main parameter to be investigated is the relative humidity. The latter is critical for works on canvas (Malowany et al., 2014) and wood (Vici et al., 2006).

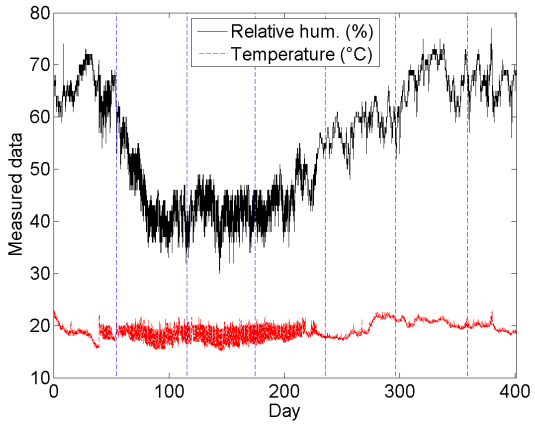

Figure 2: Change of relative humidity and temperature inside the Saint-Maurice basilica from September 7, 2013 to October 13, 2014. The dashed vertical lines correspond to transitions from even to odd months

Repeated changes of relative humidity (and temperature variations) induce a gradual relaxation of the original tension of the canvas (Berger and Russel, 1994). The latter no longer provides good support for the painted layer that deforms significantly. Being only loosely maintained the canvas and pictorial layer may start wrinkling, which eventually may initiate paint cracking (Berger and Russel, 1994). The severe conservation conditions reported in Figure 2 have consequences on the visual rendering of the painted work but more importantly they induce damage that may jeopardize its conservation. These degradation

phenomena were observed on the surface of the *Descent of the Cross* (Figure 3).

Figure 3: Damage induced by canvas wrinkling of the *Descent of the Cross* prior to its restoration

3.2. Tensioning systems

In order to avoid such phenomena to happen, two restoration routes consist of either adding interactive strainers or backing boards (Roche, 1993, 2003). The former uses springs that compensate for canvas motions. The latter consists of adding an element made of synthetic materials on the back of the strainer to create stable climatic conditions between the back of the work and the protection. In the present case, the choice of the tensioning system is driven by the strainer conservation and the location of the work in the basilica. In particular, the strainer being mounted on a wood trim so that its back is not in direct contact with the stone wall. Consequently, adding a backing wall was not considered. To limit the dimensional variations of canvas, one of the questions to be answered is whether the tensioning system can be mounted directly on the original strainer. Consequently, two different systems were evaluated.

Identical pinewood strainers were built with fixed-angles and with all edges chamfered. The strainers were 28.2×37.6 cm in size, with 3.7 cm wide and 2.8 cm thick beams. Each canvas support was cut from linen (320 g/m^2), which had been wetted and stretched three times on a large loom. The canvasses

were then sized with rabbit skin glue (10 %), primed with one layer of red ochre in linseed oil. Both size and ground were applied with a large brush. The samples were left to dry for three months before being stretched onto the strainers using two different attachment configurations. One series of paintings had a strip lining made of monofilament polyester fabric (18 g/m^2). The strainer profiles were lined with Teflon and paintings were stapled on the back face with 4-cm separation between two attachments (Figure 4(a)). Another series was stapled on the side of the strainer with the same staple separation as the other series (Figure 4(b)). Both systems were man-made at room temperature (*i.e.*, $\approx$ 22 °C) and dry conditions (*i.e.*, 35 % relative humidity). After about one hour they were put in the climatic chamber.

(a) System no. 1 (b) System no. 2

Figure 4: Studied tensioning systems

3.3. Climatic chamber

In order to study the previous tensioning systems, a home-made climatic chamber has been set up, where the humidity is varied along the day, with a quasi constant temperature of 22 °C (Figure 5(a)). It had a total volume of $2 \times 2 \times 3$ m^3 to allow two model canvas paintings to be tested and monitored at the same time. Model canvas paintings were covered with a random pattern (Figure 5(b)) and were observed using two stereocorrelation systems, each consisting of 2 Canon EOS 70D cameras with 50-mm objective lenses (Figure 5(c)).

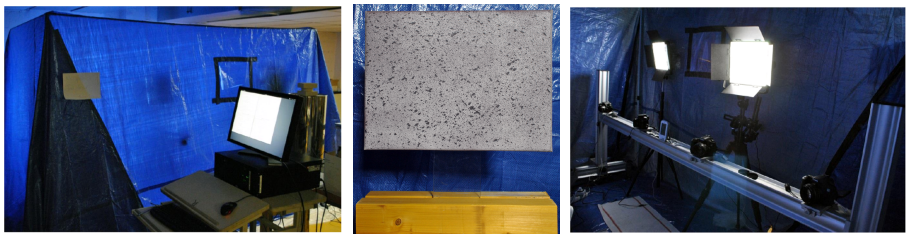

(a) (b) (c)

Figure 5: (a) Climatic chamber. (b) Model canvas painting. (c) Stereo systems

The calibration of the stereo-rigs was performed using the structure of the easel as the calibration target in order to have a 3D information, which was not available from the canvas alone (*i.e.*, quasi planar surface). Since out of plane displacements were expected to remain small, the different heights probed thanks to the easel were sufficient. The initial shape of each canvas was measured starting from a simple planar model. Figure 6 shows an example of the initial surface model and the measured shape for one of the studied canvasses. In order to measure the real shape, cubic splines (*i.e.*, 4 control points along each direction) are used, thereby leading to $4 \times 4 \times 3$ degrees of freedom. This choice is due to the fact that only small deviations from plane geometry are suspected thanks to the tensioning system.

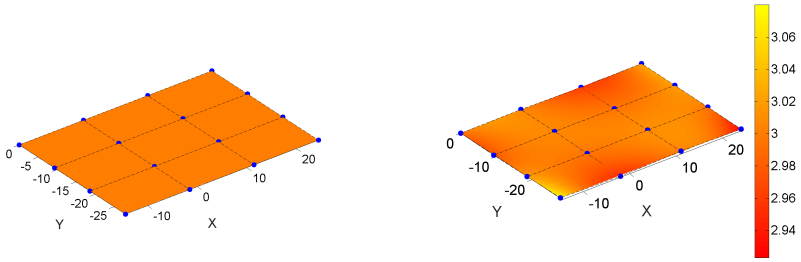

(a) (b)

Figure 6: Initial (a) and measured (b) 3D shape of one of the studied canvasses. The blue dots depict the control points of the NURBS patch for the initial shape measurement. Dimensions are expressed in cm

Each experiment lasted 21 h and was divided into 3 humidification cycles (Figure 7). The relative humidity was raised by spraying water droplets with two ultrasound Mist Maker® systems. A Proline® DH 10 dehumidifier was chosen to dry up the chamber. Each cycle consisted of:

- 20-minute humidification during which water was sprayed and a fan was on to homogenize the relative humidity level in the chamber,
- 100-minute of air circulation with the fan,
- 4-hour dehumidification during which the dehumidifier and fan are on,
- 1-h air circulation with the fan.

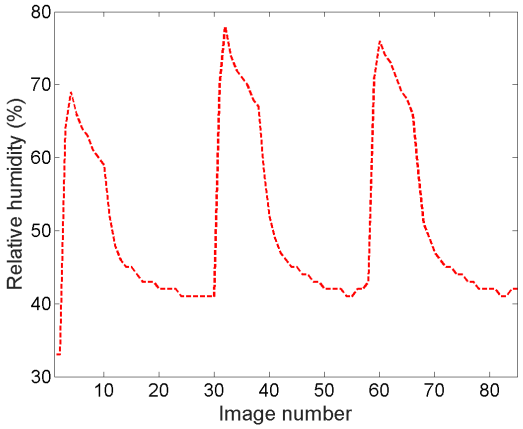

Figure 7: Relative humidity cycles for the two model canvas paintings

To monitor the relative humidity in the climatic chamber, the *same* thermo-hygrometer as for the basilica measurements was used, and was located in the center of the climatic chamber.

3.4. Analysis of two tensioning systems

By analyzing two sets of picture pairs acquired before any humidity variation the measurement resolution is estimated. In order to measure 3D displacements induced by wrinkles (*i.e.,* leading to complex shapes), 13 control points along

each direction are used, thereby leading to $13 \times 13 \times 3$ degrees of freedom. In the present case, the standard displacement uncertainty is equal to 20 μm in the out-of-plane direction, and 5 μm in in-plane directions. During the stereocorrelation analyses the levels of gray level residuals remain very low (*i.e.,* their root mean square remains of the order of 1 % of the dynamic range of the gray level pictures in the reference configuration). Consequently, the following results are deemed trustworthy.

Figure 8 shows the surface shape of two studied canvasses. In both cases small deviations to flatness are observed (*i.e.,* corresponding to the three components of displacements shown in the figure). They are due to the fact that the strainers were not perfectly flat and that the tension was applied manually. Their amplitudes remain very small, namely, less than ± 0.5 mm for system no. 2, and even lower for system no. 1. To characterize the deviation from surface flatness, the root mean square (RMS) level is also reported. The RMS flatness gap is equal to 13 μm for system no. 1 and 23 μm for system no. 2. These very small values cannot be distinguished by bare eyes but quantified via global stereocorrelation.

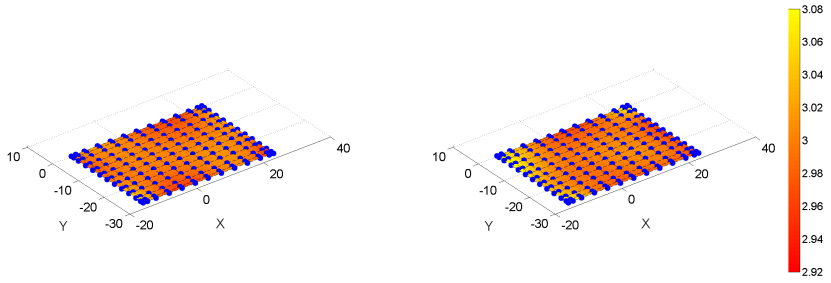

(a) System no. 1 (b) System no. 2

Figure 8: Comparison of the initial shape of canvas using two different tension devices. Dimensions are expressed in cm. The blue dots depict the control points of the NURBS patch used for the subsequent displacement measurements

Figure 9 shows pronounced canvas wrinkling due to the fact that the ten-

sioning systems cannot totally compensate for canvas extensions. In both cases wrinkles form immediately when the relative humidity is increased to 70-80 %. Moreover, when it is decreased back to 40 % levels, the canvasses instantaneously recover their initial shape. It is worth noting that more control points are used to measure the 3D deformations (Figure 8) in comparison with the initial shape (Figure 6) because of the expected deformation complexity induced by wrinkling (*i.e.,* 13×13 instead of 4×4 points).

There is a clear difference between the two solutions since system no. 1 leads to a maximum amplitude of the order of 1 mm, as opposed to the second one for which the maximum amplitude is three times the former. More importantly, the wavelength of the former is equal to $\approx 2/5$ the width of the frame. For the latter the wavelength is $\approx 2/3$ of the frame width. The RMS flatness gap is equal to 74 μm for system no. 1 and 158 μm for system no. 2.

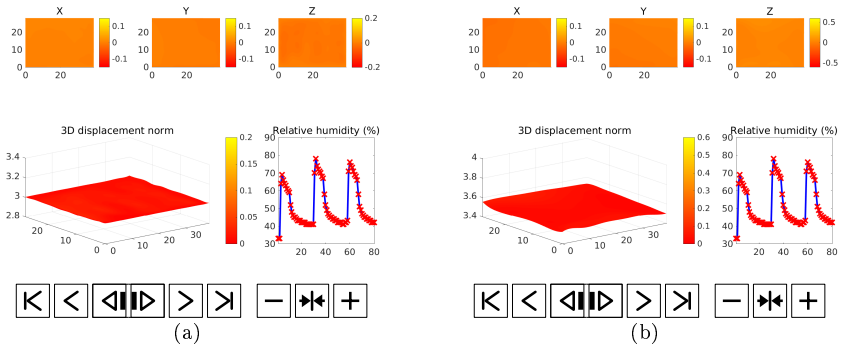

Figure 9: Comparison of the deformed shape of canvas using two different tension devices for the largest relative humidity variation. The dimensions are expressed in cm. Online version: corresponding movie for 80 analyzed steps

These comparisons were repeated five times under similar experimental conditions. The same type of results was observed (*i.e.,* number of wrinkles, deformation levels). From this analysis, system no. 1 was selected (Figure 1). The first reason was to avoid as much as possible large amplitude wrinkles, which would be detectable by bare eyes. The second reason was associated with the

Teflon tape that allows canvas tension to be as uniform as possible (Young and Hibberd, 2000), which is more difficult to ensure with system no. 2. In both cases, the wrinkles are due to the fact that the sizing absorbs water vapor from the air, which causes dimensional variations. The latter ones induce extensional strains of canvasses and all the other layers, which cannot be compensated because they are stapled on fixed stretchers.

3.5. In-situ monitoring

With the previous results, it was decided to apply the tension under given hygrometric condition (*i.e.,* the mean relative humidity monitored in Saint Maurice basilica). Similarly, the temperature was close to that of the basilica (*i.e.,* 21 °C). In order to check how the tension was applied, the *Descent of the Cross* was monitored for 24 h after being restored. Pairs of pictures are shot in 15-minute intervals for different relative humidity levels. It is worth noting that the studied work has numerous areas with very low contrast (Figure 1). Even under such demanding conditions, isogeometric stereocorrelation was run and did not induce any convergence issue. Even though the *raw* painted side has numerous low contrast zones (Figure 1), it was analyzed via (global) isogeometric stereocorrelation with no additional patterning. Thanks to the global span of NURBS interpolations these zones are part of the global analysis. The calibration of the stereo-rig was performed using the easel as calibration object. The surface model used in this case was a cubic spline (*i.e.,* single patch composed of $4 \times 4 \times 3$ degrees of freedom) with all the corresponding weights equal to 1. This choice is again dictated by the fact that the initial shape is very close to a plane. In order to better capture wrinkles, the displacement measurement is performed using a single patch made of $4 \times 7 \times 3$ degrees of freedom.

By following the same procedure as before, the standard displacement uncertainty is equal to 25 μm in the out-of-plane direction, and 5 μm in in-plane directions. The correlation residual levels observed in the present analyses were of the same order of magnitude as for model canvas paintings. This result validates the registration procedure under such challenging conditions. Figure 10

shows the displacements of the canvas and the corresponding relative humidity level. The displacement amplitudes remain less than 1 mm along the normal direction to the pictorial layer. Such small amplitudes are expected to be undetectable by bare eyes.

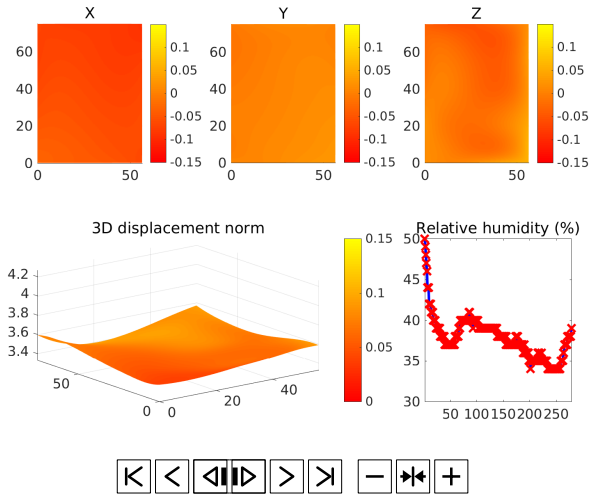

Figure 10: Displacement of the restored *Descent of the Cross* at the end of the relative humidity variation. All dimensions are expressed in cm. Online version: corresponding movie for 278 analyzed steps

After 3 days of monitoring, the in-plane displacement amplitudes are equal to 1 mm along the x (*i.e.*, warp) direction, -0.3 mm along the y (*i.e.*, weft) direction, and -0.5 mm in the out-of-plane direction. Most of the in-plane motions occur in the x-direction, in particular in the top right side that moved by 1 mm. For out-of-plane motions, their levels are very close to the resolution of the measurement technique. By analyzing the temporal deformations of canvas, two different phases are observed. Most of the displacement amplitudes occur during the early stages of relative humidity variations (*i.e.*, first five hours of the analysis) and remain less than 1 mm along the normal direction to the pictorial layer. For the last 56 hours the motions are a lot smaller and slower.

This *in-situ* analysis has allowed displacement fields to measured during canvas tensioning. Most of the motions occur during the first five hours during

which the tensions are equilibrated (Hedley, 1989). This redistribution of tensions is influenced by the relative humidity level. The restored *Descent of the Cross* has been brought back to the basilica of Saint-Maurice on December 20, 2014. The canvas tension is man-controlled each season. Having shown that stereocorrelation is a viable alternative, it could also be used to have a more quantitative assessment of *in-situ* canvas deformations.

4. Punch test on canvas

The second study was concerned with the restoration of the *Madonna with Child* (Home of Charity, Poissy, France, see Figure 11). It consisted of many steps due to the severe state of aging of the pictorial layer (*i.e.,* dusting, cleaning, unwinding, filling, unwrapping, tear consolidation, filling, varnish application, retouching (Gonnet, 2013)).

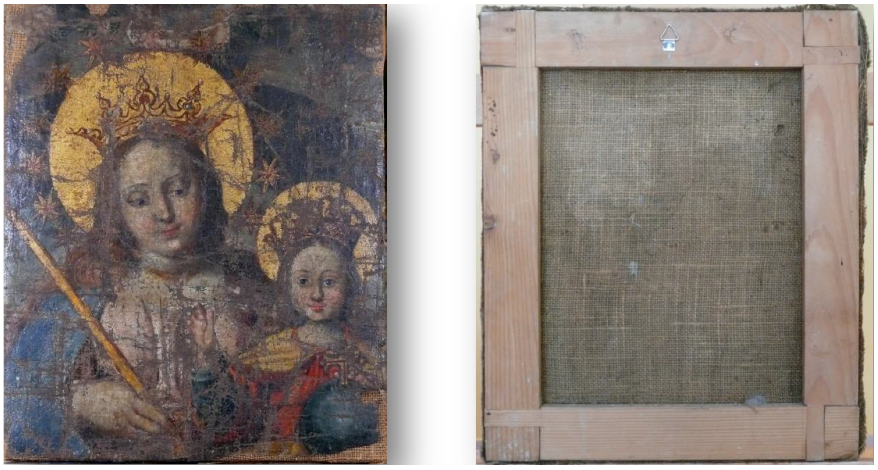

Figure 11: Front and back faces of the *Madonna with Child* prior to restoration. The size of the work is 33×39 cm

One additional issue was related to the reliability of nailed bonds of canvas on strainers. Since such type of study is destructive, it could not be performed on the actual work. Mockups were again considered for which a speckle pattern was sprayed on the back face. There are many experimental procedures to test

textiles (Lebrun et al., 2003; Cao et al., 2008; Chen, 2010). To characterize the mechanical behavior of canvas and its bond with the strainer a punch test was selected. It enabled the canvas deformation to be studied under standard bond with the strainer, namely, with nails. The external strainer size is 28×36 cm. In that case, the 3D motions are very important and the studied canvas wrinkles as more displacements are prescribed. These challenging conditions require the NURBS-based kinematics to be enriched during the different phases of displacement measurement.

Figure 12(a) shows the experimental configuration of the punch test. A sphere 50-mm in diameter made of steel was selected. It was moved at a speed of 50 μm/s by the actuator of the servohydraulic testing machine. As in the previous study, a model canvas painting was considered. It could be speckled with black and white paint on its back face (Figure 12(b)). The loaded strainer was simply supported with respect to the frame of the testing machine. The stereo-system consisted of 2 Canon EOS 60D cameras with 50-mm objective lenses. It was located above the tested canvas. The interframe time was 10 s.

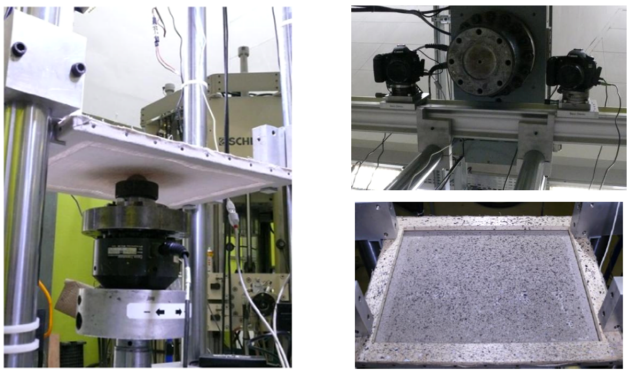

(a) (b)

Figure 12: (a) Punch test. (b) Stereo-rig and speckled canvas

Contrary to the previous cases, very large deformations were expected, and the frame height was not sufficient to ensure a good calibration to cover the whole displacement amplitude. Consequently, an open book target was used to

calibrate the stereo system (Figure 13). One of its advantages also lies in the fact that being non planar, only one set of images is sufficient for calibration purposes (Besnard et al., 2010).

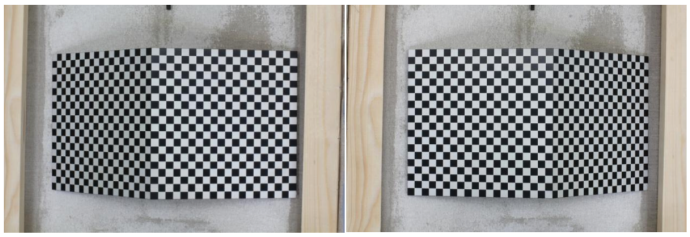

Figure 13: Image pair that was used for the calibration of the stereo-rig with an open book target

During this type of experiments, the shape of the canvas is significantly changing from a simple rectangular plate (shown in Figure 14), to a much more complex geometry. To measure the initial 3D shape, 4×4 control points are chosen (for the same reasons as before). However, the deformed shape asked for additional degrees of freedom, which are gradually added.

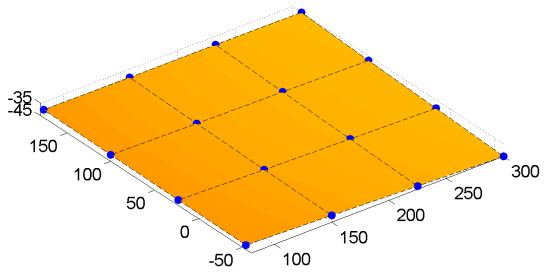

Figure 14: Initial canvas shape. All dimensions are expressed in mm. The blue dots depict the control points of the NURBS patch

The refinement procedure used herein is very simple. At specific intervals,

2×2 control points are added to the knot vector (one on each side of the central value 0.5 to preserve symmetry), thus creating new knot spans in knot vector, and new 'elements' inside the NURBS patch. In the present case, 2 new knot spans (thus control points) are added every 5 image. Consequently, the surface model is refined starting from the center and moving to the edges. This kind of strategy (*i.e.,* knot refinement) is a standard way to increase the number of degrees of freedom without increasing the degree of the solution (Cottrell et al., 2009) (*i.e.,* in a similar way as the so-called h-refinement technique in finite element methods (Zienkievicz and Taylor, 1989)). It also preserves maximum continuity inside the patch (*i.e.,* through 'elements'), thus allowing smooth solutions to be accurately captured. Figure 15(a) shows the change of the number of degrees of freedom as more images are analyzed. The total number of unknowns is thus increased from 48 to nearly 2,700 at the end of the analysis. The procedure chosen herein follows the load increase during the test (Figure 15(b)). The stereocorrelation analysis was not conducted until the very end of the experiment because severe canvas damage occurred after the last studied image pair.

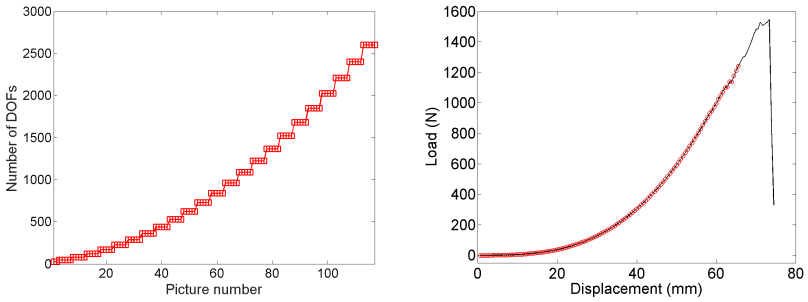

(a) (b)

Figure 15: (a) Change of number of kinematic degrees of freedom with the image number during the punch test. (b) Load displacement curve of the punch test (the open circles correspond to the analyzed picture pairs)

Figure 16(a) shows the change of root mean square registration residual as

a function of the analyzed picture. There is a clear decrease of the level at convergence in comparison with the initial level (*i.e.*, no displacement corrections have been performed and the displacement field of the previous image pair is used as initial guess). This general trend proves that the algorithm was able to capture meaningful displacement fields. This result validates the enrichment strategy of the measured kinematics. Some spikes are noted at the end of the experiment. They are due to illumination variations that are more pronounced.

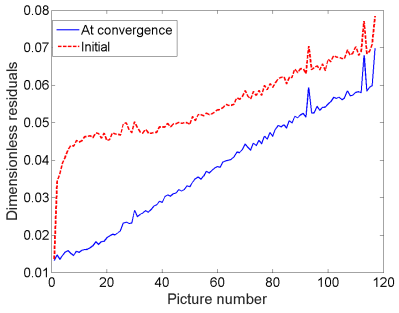

(a)

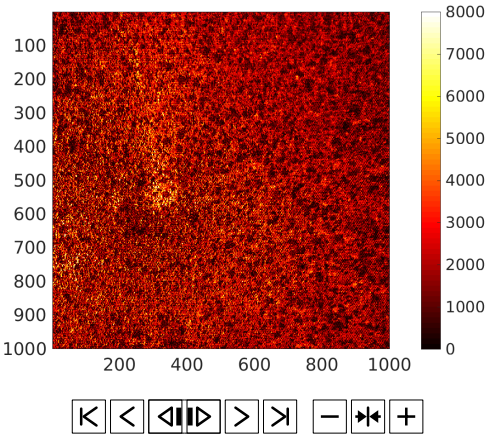

(b)

Figure 16: (a) Change of the RMS correlation residuals with the image number during the punch test. (b) Gray level residual field for the peak load (the dynamic range of the pictures is 16 bits). Online version: corresponding movie for 117 analyzed steps

Even though the measurements are deemed trustworthy, there still is a grad-

ual increase of the RMS levels. By examining the residual fields (Figure 16(b)) it is observed that as the sphere displacement level increases, the registration quality degrades in the vicinity of the sphere pole. Yarn motions occur, which are not compatible with the chosen kinematics. Moreover, at the end of the experiment, some yarns presumably fail. This (discontinuous) mechanism cannot be captured by the (continuous) kinematic basis used herein (NURBS). However, it is detected by the correlation residuals.

The deformed shape of the tested canvas is shown in Figure 17 in addition to the out-of-plane displacement. As more displacements are applied to the sphere, more wrinkles appear. These wrinkles come from the method used to attach the canvas to the strainer (*i.e.,* with nails). As there is a finite number of nails on the strainer, the tension in the canvas is (spatially) oscillating thereby inducing wrinkles of the canvas. At the end of the experiment, the nailed bond was still working properly while canvas degradation occurred (see Figures 15(b) and 16(b)). This observation validates the nail spacing chosen in the present study.

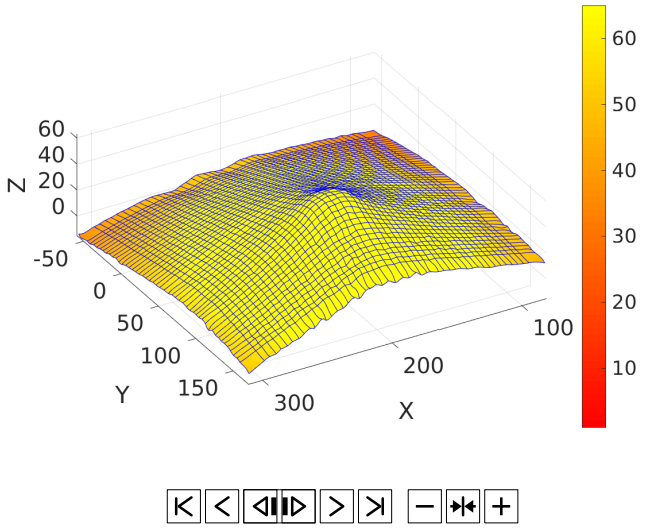

Figure 17: Deformed canvas and out-of-place displacements via isogeometric stereocorrelation for the peak load. All dimensions are expressed in mm. The blue lines depict the knot spans (similar to elements in a finite element formulation) of the NURBS formulation. Online version: corresponding movie for 117 analyzed steps

5. Conclusion

Isogeometric stereocorrelation was successfully applied to study canvas wrinkling. This deformation mechanism is to be reduced as much as possible for painted works on canvas. Conversely, in a punch test wrinkling will occur and needs to be assessed. Because higher order kinematics was sought, NURBS-based stereocorrelation was considered for the initial 3D shape and its deformation induced either by relative humidity variations or during a punch test.

The first case was associated with the restoration of the *Descent of the Cross* for which the tensioning system had to be studied. Due to significant humidity variations, canvas tension varied, which may lead to wrinkles that are detrimental to the visual quality and aging of the work. Two tensioning systems have been investigated on model canvas paintings that are submitted to humidity variations. The 3D shapes and motions were measured via isogeometric stereocorrelation. In the present case, the studied canvasses were patterned with random speckles. The two tensioning system did not lead to the same curvature fields. Once the system was selected for the *Descent of the Cross*, its 3D shape and motions were also monitored via isogeometric stereocorrelation to validate the chosen technical solution even though the painted layer contained areas with very low contrast (the whole pictorial layer could be analyzed thanks to the global support of NURBS).

The second study was concerned with the restoration of the *Madonna with Child*. The mechanical characterization of canvas and its bond was performed via a punch test on a model canvas nailed on its strainer. In that case, the 3D motions were very important and the studied canvas wrinkled as more displacements were prescribed. These challenging conditions required the kinematic description based on NURBS to be enriched during the different phases of measurement. Further, the analysis of the registration residuals showed that early stages of yarn motions and breakage are detected.

These two case studies prove the feasibility of isogeometric stereocorrelation to be applied in the context of restoration of canvas paintings. Thanks to its

versatility, it could be adapted to the two studied situations that induced either very small deformations of canvas, very large levels, or low contrasted works. If more local analyses are required, namely, the displacements at the yarn levels, the same formalism can be used by considering the NURBS or FE model of canvas (Naouar et al., 2014).

Acknowledgements

This work was partially supported under the PRC Composites, French research project funded by DGAC, involving SAFRAN Group, ONERA and CNRS.

References

Ambrosini, D., Paoletti, D., Galli, G., 2008. Lasers in the Conservation of Artworks. CRC Press. chapter Chapter 64. Integrated digital speckle based techniques for artworks monitoring. pp. 399–405.

Beaubier, B., Dufour, J., Hild, F., Roux, S., Lavernhe-Taillard, S., Lavernhe-Taillard, K., 2014. CAD-based calibration of a 3D-DIC system: Principle and application on test and industrial parts. Exp. Mech. 54, 329–341.

Berger, G., Russel, W., 1994. Interaction between canvas and paint film in response to environmental changes. Stud. Conservation 39, 73–86.

Besnard, G., Lagrange, J., Hild, F., Roux, S., Voltz, C., 2010. Characterization of necking phenomena in high speed experiments by using a single camera. EURASIP J. Im. Video. Proc. 2010, 15 p.

Cao, J., Akkerman, R., Boisse, P., Chen, J., Cheng, H., de Graaf, E., Gorczyca, J., Harrison, P., Hivet, G., Launay, J., Lee, W., Liu, L., Lomov, S., Long, A., de Luycker, E., Morestin, F., Padvoiskis, J., Peng, X., Sherwood, J., Stoilova, T., Tao, X., Verpoest, I., Willems, A., Wiggers, J., Yu, T., Zhu, B., 2008. Characterization of mechanical behavior of woven fabrics: Experimental methods and benchmark results. Compos. Part A 39, 1037–1053.

Chen, X. (Ed.), 2010. Modelling and Predicting Textile Behaviour. Woodhead Publishing, Oxford (UK).

Cottrell, J., Hughes, T., Bazilevs, Y., 2009. Isogeometric Analysis: Toward Integration of CAD and FEA. Wiley.

Dubreuil, L., Dufour, J.E., Quinsat, Y., Hild, F., 2016. Mesh-based shape measurements with stereocorrelation. Exp. Mech. 56, 1231–1242.

Dufour, J., Beaubier, B., Roux, S., Hild, F., 2014. Displacement measurement using CAD-based stereo-correlation with meshes, in: ICEM conference.

Dufour, J.E., Beaubier, B., Hild, F., Roux, S., 2015a. CAD-based displacement measurements. Principle and first validations. Exp. Mech. 55, 1657–1668.

Dufour, J.E., Hild, F., Roux, S., 2015b. Shape, Displacement and Mechanical Properties from Isogeometric Multiview Stereocorrelation. J. Strain Analysis 50, 470–487.

Dulieu-Barton, J., Dokos, L., Eastop, D.E., Lennard, F.J., Chambers, A., Sahin, M., 2005. Deformation and strain measurement techniques for the inspection of damage in works of art. Rev. Conserv. 6, 61–71.

Dureisseix, D., Colmars, J., Baldit, A., Morestin, F., Maigre, H., 2011. Follow-up of a panel restoration procedure through image correlation and finite element modeling. Int. J. Solids Struct. 48, 1024–1033.

Faugeras, O., Luong, Q., Maybank, S., 1992. Camera self-calibration: Theory and experiments, in: Proc. 2nd ECCV, Springer-Verlag. pp. 321–334.

Faugeras, O., Toscani, G., 1987. Camera calibration for 3D computer Vision, in: International Workshop on Machine Vision and Machine Intelligence, pp. 240–247.

Fusiello, A., 2000. Uncalibrated euclidean reconstruction: a review. Im. vis. comput. 18, 555–563.

Gavrilov, D., Maev, R., Almond, D., 2014. A review of imaging methods in analysis of works of art: Thermographic imaging method in art analysis. Canad. J. Phys. 92, 341–364.

Gonnet, E., 2013. Restauration d'une Vierge à l'Enfant, la redécouverte d'une œuvre grâce à sa restauration. Technical Report. Ecole de Condé, Paris.

Grau, S., 2014. Conservation et restauration de la Descente de Croix conservée dans le chœur de la basilique de Saint-Maurice en Valais. Technical Report. Ecole de Condé, Paris.

Hedley, G., 1989. Relative humidity and the stress/strain response of canvas paintings: uniaxial measurements of naturally aged samples. Stud. Conservation 34, 133–148.

James, A., Gibbs, S., Sloan, M., Erickson, J. Diggs, J., 1983. Radiographic techniques to evaluate paintings. Am. J. Roentgenol. 140, 215–220.

Khennouf, D., Dulieu-Barton, J., Chambers, A., Lennard, F., Eastop, D., 2010. Assessing the feasibility of monitoring strain in historical tapestries using digital image correlation. Strain 46, 19–32.

Lebrun, G., Bureau, M., Denault, J., 2003. Evaluation of bias-extension and picture-frame test methods for the measurement of intraply shear properties of pp/glass commingled fabrics. Compos. Struct. 61, 341–352.

Lucas, B., Kanade, T., 1981. An iterative image registration technique with an application to stereo vision, in: 7th International Joint Conference on Artificial Intelligence, pp. 674–679.

Malowany, K., Tyminska-Widmer, L., Malesa, M., Kujawinska, M., Targowski, P., Rouba, B., 2014. Application of 3D digital image correlation to track displacements and strains of canvas paintings exposed to relative humidity changes. Appl. Opt. 53, 1739–49.

Mudge, M., Schroer, C., Earl, G., Martinez, K., Pagi, H., Toler-Franklin, C., Rusinkiewicz, S., Palma, G., Wachowiak, M., Ashley, M., Matthews, N., Noble, T., Dellepiane, M., . Principles and practices of robust, photography-based digital imaging techniques for museums, in: 11th International Symposium on Virtual reality, Archaeology and Cultural Heritage VAST.

Naouar, N., Vidal-Sallé, E., Schneider, J., Maire, E., Boisse, P., 2014. Meso-scale FE analyses of textile composite reinforcement deformation based on X-ray computed tomography. Comp. Struct. 116, 165–176.

Piegl, L., Tiller, W., 1997. The NURBS Book - 2nd Edition. Springer.

Remondino, F., Rizzi, A., Barazzetti, L., Scaioni, M., Fassi, F., Brumana, R., Pelagotti, A., 2011. Review of geometric and radiometric analyses of paintings. The Photogrammetric Record 26, 439–461.

Roche, A., 1993. Influence du type de châssis sur le vieillissement mécanique d'une peinture sur toile. Stud. Conservation 38, 17–24.

Roche, A., 2003. Comportement mécanique des peintures sur toiles. CNRS Editions, Paris (France). chapter Application aux mesures de conservation et aux traitements. pp. 169–183.

Salvi, J., Armague, X., Battle, J., 2002. A comparative review of camera calibrating methods with accuracy evaluation. Pattern Recog. 35, 1617–1635.

Sfarra, S., Ibarra-Castanedo, C., Ambrosini, D., Paoletti, D., Bendada, A., Maldague, X., 2014. Non-destructive testing techniques to help the restoration of frescoes. Arab. J. Sci. Eng. 39, 3461–3480.

Sutton, M., 2013. Computer vision-based, noncontacting deformation measurements in mechanics: A generational transformation. Appl. Mech. Rev. 65, 050802.

Sutton, M., Orteu, J., Schreier, H., 2009. Image correlation for shape, motion and deformation measurements: Basic Concepts, Theory and Applications. Springer, New York, NY (USA).

Vici, P.D., Mazzanti, P., Uzielli, L., 2006. Mechanical response of wooden boards subjected to humidity step variations: climatic chamber measurements and fitted mathematical models. J. Cultur. Heritage 7, 37–48.

Weng, J., Cohen, P., Herniou, M., 1992. Camera calibration with distortion models and accuracy evaluation. IEEE Trans. Pattern Anal. Machine Intell. 14, 965–980.

Young, C., Hibberd, R., 2000. The role of canvas attachments in the strain distribution and degradation of easel paintings. Stud. Conservation 54, 212–220.

Zhang, Z., 2000. A flexible new technique for camera calibration. IEEE Trans. Pattern Anal. Machine Intell. 22, 1330–1334.

Zienkievicz, O., Taylor, R., 1989. The Finite Element Method. 4th edition, McGraw-Hill, London (UK).